

# Halt the Hallucination: Decoupling Signal and Semantic OOD Detection Based on Cascaded Early Rejection

Ningkang Peng<sup>1</sup>, Chuanjie Cheng<sup>1</sup>, Jingyang Mao<sup>1</sup>, Xiaoqian Peng<sup>2</sup>, Feng Xing<sup>1</sup>,  
Bo Zhang<sup>1,\*</sup>, Chao Tan<sup>1,\*</sup>, Zhichao Zheng<sup>1,\*</sup>, Peiheng Li<sup>1,\*</sup>, Yanhui Gu<sup>1\*</sup>

<sup>1</sup>School of Computer and Electronic Information, Nanjing Normal University, China

<sup>2</sup>School of Artificial Intelligence and Information Technology, Nanjing University of Chinese Medicine, China

zhangbo@nnu.edu.cn, {tutu\_tanchao, zheng\_zhichao}@163.com, leeess@nnu.edu.cn, gu@njnu.edu.cn,

## Abstract

Efficient and robust Out-of-Distribution (OOD) detection is paramount for safety-critical applications. However, existing methods still execute full-scale inference on low-level statistical noise. This computational mismatch not only incurs resource waste but also induces semantic hallucination, where deep networks forcefully interpret physical anomalies as high-confidence semantic features. To address this, we propose the **Cascaded Early Rejection (CER)** framework, which realizes hierarchical filtering for anomaly detection via a coarse-to-fine logic. CER comprises two core modules: 1) **Structural Energy Sieve (SES)**, which establishes a non-parametric barrier at the network entry using the Laplacian operator to efficiently intercept physical signal anomalies; and 2) the **Semantically-aware Hyperspherical Energy (SHE) detector**, which decouples feature magnitude from direction in intermediate layers to identify fine-grained semantic deviations. Experimental results demonstrate that CER not only reduces computational overhead by 32% but also achieves a significant performance leap on the CIFAR-100 benchmark: the average FPR95 drastically decreases from 33.58% to 22.84%, and AUROC improves to 93.97%. Crucially, in real-world scenarios simulating sensor failures, CER exhibits performance far exceeding state-of-the-art methods. As a universal plugin, CER can be seamlessly integrated into various SOTA models to provide performance gains.

## 1 Introduction

Deep learning models have achieved remarkable success in safety-critical domains such as autonomous driving [Huang *et al.*, 2021] and medical diagnosis. However, these models are typically trained under a closed-world assumption and often yield overconfident, erroneous predictions when encountering unknown Out-of-Distribution (OOD) samples in real-

\*Corresponding authors.

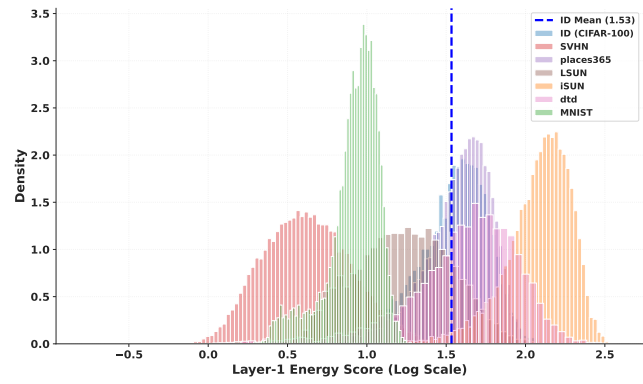


Figure 1: **High-Frequency Energy Distribution Comparison.** The histogram illustrates the distinct separation between ID data (CIFAR-100) and various OOD datasets. Far-OOD samples like SVHN and MNIST exhibit significantly lower energy.

world open scenarios. While existing OOD detection methods have made significant strides in performance, most are confined to a post-hoc processing paradigm at the network’s final layer.

This paradigm faces a severe **Computational Mismatch** in practical deployment: whether the input is a complex semantic object or simple sensor noise or physical perturbation, the model is compelled to execute full-path deep feature abstraction.[Kaya *et al.*, 2019] This computational mismatch not only causes severe resource waste but, more critically, induces **Semantic Hallucination**. When non-semantic statistical noise is forcefully fed into deep networks, complex non-linear transformations over-interpret these meaningless signals, generating high-confidence misjudgments. *For instance, in our preliminary experiments, a model pre-trained on CIFAR-100 would mistake simple MNIST handwritten digits for high-confidence semantic categories.* [Teerapittayanon *et al.*, 2016] This demonstrates that deep feature extraction is not only redundant but dangerous for low-level noise.

To alleviate computational bottlenecks, multi-exit architectures (e.g., MOOD) attempt to utilize intermediate layer confidence for early exiting. However, such methods often fall into the trap of **Inductive Bias Mismatch**. They forcibly assume that shallow features can simultaneously support ID classification and OOD detection. However, shallow layers, lacking global context, cannot make rigorous semantic deci-

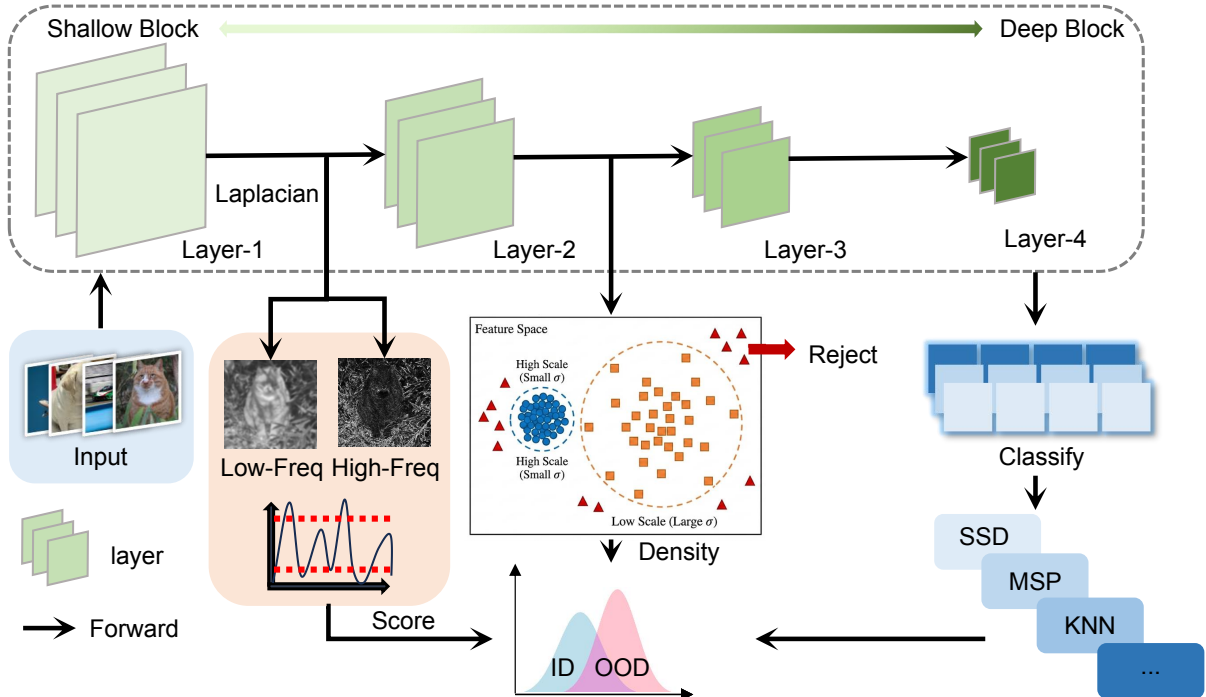


Figure 2: Overview of proposed CER framework. The CER framework implements an adaptive, multi-stage OOD detection mechanism by integrating physical representation analysis with deep semantic discrimination. Rather than relying on a single judgment at the final layer of the network, the framework deploys multiple specialized detection heads at varying network depths to progressively reject OOD samples based on their individual complexity.

sions, leading models to sacrifice detection rigor for speed.

To this end, we propose the **Cascaded Early Rejection (CER)** framework. We reformulate efficient OOD detection as a cascaded inference task under computational constraints and advocate for thoroughly decoupling signal rejection from semantic classification. Inspired by the spectral energy distribution laws of natural images [Wang *et al.*, 2020], as shown in Figure 1, we utilize the Laplacian operator at the network entry to capture high-frequency structural anomalies, blocking deep hallucinations induced by non-semantic noise at the source. For samples that bypass the physical sieve, we utilize hyperspherical geometric projection at the semantic transition layer to decouple feature magnitude from direction, [Hasnat *et al.*, 2017] eliminating interference from unstable activation scales and discriminating solely based on semantic directional consistency.

The main contributions of this paper are as follows:

1. **Paradigm Shift:** We reveal the overlooked issues of computational mismatch and inductive bias mismatch in existing OOD detection and propose a new paradigm of decoupling shallow signal rejection from deep semantic discrimination.
2. **Technical Innovation:** We introduce the synergistic SES module and SHE model. The former rapidly filters texture artifacts via physical statistical laws, while the latter ensures the semantic rigor of intermediate layer decisions via hyperspherical projection. While reducing computational overhead by 32%, we significantly optimize the FPR95 on CIFAR-100 from 33.58% to 22.84%.

3. **Safety Enhancement in Extreme Environments:** We conducted in-depth testing on real-world noise environments such as **Sensor Failure**. Results show that CER demonstrates robustness far exceeding existing SOTA methods, effectively preventing system crashes caused by low-level signal anomalies.

4. **Highly Universal Plugin Design:** CER can be seamlessly integrated into various mainstream backbone networks, endowing models with efficient and safe detection capabilities without the need for complex retraining.

## 2 Related Work

**Out-of-Distribution Detection.** Existing OOD detection methodologies generally fall into two primary categories: score-based and distance-based approaches. Score-based methods focus on designing specific metrics to discriminate between ID and OOD samples. Hendrycks & Gimpel established a baseline with MSP, directly utilizing the Maximum Softmax Probability as a confidence score. Subsequently, ODIN [Liang *et al.*, 2018] introduced temperature scaling and input preprocessing to amplify the distributional divergence between ID and OOD data. [Liu *et al.*, 2020] demonstrated that the Energy Score theoretically aligns better with the probability density than softmax confidence. Furthermore, methods like ReAct [Sun *et al.*, 2021] and ASH [Djuricic *et al.*, 2023] suppress anomalous

activations from OOD samples by rectifying or pruning feature activations. Distance-based methods, conversely, leverage geometric statistics within the deep feature space. A quintessential example is the Mahalanobis distance [Lee *et al.*, 2018], which models ID features as multivariate Gaussian distributions and measures the distance between test samples and class centroids. Additionally, non-parametric approaches based on KNN have proven effective in handling complex distributions. However, existing post-hoc paradigms universally suffer from a computational mismatch. Due to their strict reliance on deep semantic features, even simple physical noise is compelled to undergo expensive, full-network inference. This not only results in computational waste but also forces the network to over-interpret low-level anomalies [Chen and Wang, 2025], thereby inducing semantic hallucination [Peng *et al.*, 2025].

**Dynamic Inference & Early Exiting.** To alleviate the computational burden of deep models, dynamic inference architectures have been extensively studied. Classic methods such as BranchyNet [Teerapittayanon *et al.*, 2016] and MSD-Net [Huang *et al.*, 2018] insert auxiliary shallow classifiers at intermediate layers, allowing easy samples to exit early once a confidence threshold is met. [Zeiler and Fergus, 2014] MOOD [Lin *et al.*, 2021] further extended this paradigm to OOD detection, [Nguyen *et al.*, 2015] utilizing intermediate classification confidence to intercept out-of-distribution samples early. [Scardapane *et al.*, 2020] However, such methods suffer from an inductive bias mismatch. Shallow features inherently lack the semantic depth required for fine-grained classification; forcing intermediate layers to perform classification predictions often leads to unreliable decisions, essentially sacrificing rigor for speed. [Li and others, 2023] In contrast, our proposed CER framework redefines the objective of early exiting. Rather than forcing intermediate layers to predict classes, we reduce the task to anomaly rejection.

### 3 Method

#### 3.1 The CER Framework

Motivated by the efficiency of multi-exit architectures, we propose the **Cascaded Early Rejection (CER)** framework [Bernhard and others, 2021]. We formulate the model as a sequential cascade of  $K$  rejection modules  $\mathcal{M} = \{M_1, \dots, M_K\}$ . Rather than generating parallel predictions, this framework produces a chain of conditional gating decisions.

Let  $\mathbf{z}_0$  denote the raw input image  $x$ . The feature extraction at the  $i$ -th stage is recursively defined as:

$$\mathbf{z}_i = f_i(\mathbf{z}_{i-1}; \theta_i), \quad i \in \{1, \dots, K\}, \quad (1)$$

where  $f_i(\cdot; \theta_i)$  represents the  $i$ -th neural block parameterized by  $\theta_i$ .

Within the CER framework, we introduce intermediate rejection modules at varying levels to enable dynamic, coarse-to-fine OOD inference. We formally define the Rejection Gate  $G_i(\mathbf{z}_i)$  at stage  $i$  as a binary indicator:

$$G_i(\mathbf{z}_i) = \begin{cases} 1, & \text{if } S_i(\mathbf{z}_i) \in \mathcal{A}_i \\ 0, & \text{if } S_i(\mathbf{z}_i) \notin \mathcal{A}_i \end{cases} \quad (2)$$

Here,  $S_i(\cdot)$  is the stage-specific scoring function, and  $\mathcal{A}_i$  denotes the ID-derived acceptance region.

Crucially, this training-free design formalizes the global inference as a conditional execution chain:

$$\text{Output}(x) = \begin{cases} \perp, & \text{if } \exists i < K, G_i(\mathbf{z}_i) = 0 \\ f_K(\mathbf{z}_K), & \text{otherwise} \end{cases} \quad (3)$$

where  $\perp$  denotes the rejection state. This formulation implies that the final semantic classifier  $f_K$  is triggered *if and only if* the sample successfully traverses all  $K - 1$  rejection modules. [Wolczyk and others, 2021]

#### 3.2 Physical-aware Structural Energy Screening

Deep neural networks often exhibit a texture bias, assigning disproportionately high confidence to statistical anomalies. While natural images typically adhere to the  $1/f^\alpha$  spectral laws, OOD samples (e.g., chaotic noise) deviate significantly from these regularities. To efficiently intercept such low-level physical anomalies without the computational overhead of the Fourier Transform, we introduce the Structural Energy Screening (SES) module.

We leverage the Laplacian operator as a computationally efficient, isotropic proxy for high-frequency spectral energy. Given the shallow feature map  $\mathbf{z}_1 \in \mathbb{R}^{C \times H \times W}$ , we perform depth-wise convolution with a fixed Laplacian kernel  $\mathbf{K}_{Lap}$  to extract channel-wise residuals:

$$\mathbf{H}_{freq} = |\mathbf{z}_1 * \mathbf{K}_{Lap}|, \quad (4)$$

where  $\mathbf{H}_{freq}$  quantifies the local spectral singularities, and  $|\cdot|$  denotes the element-wise absolute value. In the frequency domain, the Laplacian response approximates the integrated power spectrum weighted by spatial frequency  $\omega$ . Formally, the captured energy satisfies:

$$\mathbb{E}[|\mathbf{H}_{freq}|^2] \propto \int \omega^2 |\mathcal{F}(\mathbf{z}_1)(\omega)|^2 d\omega.$$

This analytical result confirms that SES acts as a high-pass filter, selectively targeting the high-frequency violations typical of OOD noise.

While  $\mathbf{H}_{freq}$  captures local singularities, aggregating these responses requires careful design. Standard Global Average Pooling (GAP) treats all channels equally, inevitably diluting local physical anomalies with background signals.

To address this, we propose an **Adaptive Top-K Spectral Pooling** strategy. We focus on the most energetic frequency bands rather than the global average. The final structural energy score  $S_1(\mathbf{z}_1)$  is formulated as:

$$\begin{aligned} S_1(\mathbf{z}_1) &= \frac{1}{K} \sum_{c \in \Omega_K} \log \left( \frac{1}{HW} \sum_{h,w} H_{freq}^{(c)}(h,w) + \epsilon \right) \\ &= -\langle E(\mathbf{z}_1; c) \rangle_{c \in \Omega_K} \\ &= \log \Psi(\mathbf{z}_1; \Omega_K) \end{aligned} \quad (5)$$

where  $H$  and  $W$  denote the height and width of the feature map, respectively. The operator  $\langle \cdot \rangle_{c \in \Omega_K}$  denotes the *ensemble average* over the top- $K$  most energetic channels,

and  $\Psi(z_1; \Omega_K)$  is defined as the *global confidence level* of the physical sieve. Specifically,  $E(z_1; c)$  represents the channel-wise energy function derived from the spatially averaged high-frequency response, while the log-transformation  $\log \Psi(\cdot)$  effectively linearizes the spectral power to suppress stochastic background noise.

Our derivation stems from the *Spectral Sparsity Prior*: physical anomalies typically manifest in only a sparse subset of channels  $\mathcal{C}_{\text{anom}}$  (i.e.,  $|\mathcal{C}_{\text{anom}}| \ll C$ ). Under the standard GAP, the anomaly signal is inevitably diluted by the dominant background responses. To quantify the degree of anomaly signal enhancement, we formally define the **Spectral Contrast Gain** ( $G$ ) as:

$$G \triangleq \frac{\exp(S_1(z_1))}{\frac{1}{C} \sum_{c=1}^C \exp(e^{(c)})} \quad (6)$$

where  $S_1(z_1)$  denotes the activation strength of the Top-1 channel, and  $e^{(c)}$  represents the energy response of the  $c$ -th channel. The physical significance of  $G$  lies in its ability to directly characterize the ratio between the strongest single-channel anomaly activation and the ensemble average of the background noise.

Through this formulation, our SES can explicitly extract sparse anomalous features from the background. Consequently, even in the presence of significant texture bias, the anomaly signal remains distinguishable and is prevented from being submerged by the global averaging operation, provided that  $G$  is sufficiently large.

### 3.3 Semantically-aware Hyperspherical Energy

Inspired by related work on multi-exit architectures, we propose an energy-based OOD detection method. Specifically [Wang and Zhang, 2025], we derive the fundamental energy score based on the concept of exit classifiers:

$$E(z) = -\log \sum_{j=1}^C e^{f^{(j)}(z, \theta)} \quad (7)$$

where  $C$  is the number of classes for in-distribution (ID) data,  $f^{(j)}(z, \theta)$  denotes the logit output for the  $j$ -th class, and  $\theta$  represents the model parameters.

In general analysis, if we consider the dominant role of feature magnitude, the energy function can be expanded as:

$$E(z) = -\log \sum_{c=1}^C \exp(\alpha_c \|z\| + b_c) \quad (8)$$

$$= -\log (C \cdot \exp(\alpha \|z\|)) \quad (9)$$

$$= -\alpha \|z\| - \log C \quad (10)$$

where we assume that the feature magnitude  $\|z\|$  solely determines  $f^{(c)}(z)$ , and the weight gains  $\alpha$  are identical across all classes with zero bias, making both  $\alpha$  and  $C$  constants.

However, at intermediate layers of a neural network, relying solely on or even including magnitude information for decision-making is unreliable. Intermediate layers exhibit extremely strong responses to low-level physical attributes such as local contrast, sharp edges, and high-frequency noise.

These physical features trigger massive feature magnitudes  $\|z\|$ , yet they carry no semantic information useful for distinguishing ID from OOD data.

According to the derivation in Eq. (10), as long as  $\|z\|$  is sufficiently large, the energy will be extremely low. This creates a paradox: an OOD sample filled with meaningless high-frequency noise appears more normal to the energy model than an ID sample with a smaller feature magnitude.

To address this issue, we introduce the concept of class prototypes and hyperspherical embedding into the intermediate energy score. First, we define the class prototype  $\mu_k$  as:

$$\mu_k = \frac{\sum_{n=1}^{N_k} \omega_{n,k} \cdot z_{n,k}}{\left\| \sum_{n=1}^{N_k} \omega_{n,k} \cdot z_{n,k} \right\|_2} \quad (11)$$

where  $z_{n,k}$  is the feature vector of the  $n$ -th training sample belonging to the  $k$ -th class extracted from an intermediate layer,  $N_k$  is the total number of samples in that class, and  $\omega_{n,k}$  is the weight coefficient for the  $n$ -th sample, used to measure its semantic representativeness.

Next, by leveraging hyperspherical embedding [Ming and Li, 2023], we transform the energy score into a metric focused on semantic information:

$$f^{(j)}(z, \theta) = \|w_j\| \|z\| \cos(\theta_{z, w_j}) + b_j \quad (12)$$

$$= \kappa_j \cdot \frac{z^\top \mu_j}{\|z\|} \quad (13)$$

where  $\cos(\theta_{z, w_j})$  represents the semantic consistency (direction) between the feature and the class, and  $\kappa_j$  denotes the intra-class angular dispersion calibration factor. [Smith and Li, 2025] Based on this, we arrive at the final **semantically-aware hyperspherical energy** formula:

$$E(z) = -\log \sum_{j=1}^C \exp \left( \kappa_j \cdot \frac{z^\top \mu_j}{\|z\|} \right) \quad (14)$$

By introducing the  $L_2$  normalization constraint (the  $\|z\|$  in the denominator), this formula achieves complete decoupling of feature intensity from directional semantics. It forces the model to make judgments based solely on the semantic matching between the feature and the class prototypes, thereby fundamentally suppressing semantic hallucinations caused by magnitude bias.

## 4 Experiments

### 4.1 Experimental Setup

**Datasets.** We establish **CIFAR-10** and **CIFAR-100** [Krizhevsky *et al.*, 2009] as the in-distribution (ID) datasets. For out-of-distribution (OOD) evaluation, we utilize a comprehensive suite of natural image datasets, including **SVHN** [Netzer *et al.*, 2011], **Places365** [Zhou *et al.*, 2017], **LSUN** (Crop and Resize) [Yu *et al.*, 2015], **iSUN** [Xu *et al.*, 2015], **Textures** [Cimpoi *et al.*, 2014], and **MNIST** [LeCun *et al.*, 1998]. Consistent with standard protocols, all OOD images are resized to  $32 \times 32$  to match the ID resolution.

Methods	OOD Datasets													
	SVHN		MNIST		Places365		LSUN		iSUN		Textures		Average	
	FPR95↓	AUROC↑	FPR95↓	AUROC↑	FPR95↓	AUROC↑	FPR95↓	AUROC↑	FPR95↓	AUROC↑	FPR95↓	AUROC↑	FPR95↓	AUROC↑
MSP	78.89	79.80	88.23	78.25	84.38	74.21	83.47	75.28	84.61	74.51	86.51	72.53	84.35	75.76
ODIN	70.16	84.88	92.33	71.54	82.16	75.19	76.36	80.10	79.54	79.16	85.28	75.23	80.97	77.68
Energy	66.91	85.25	91.49	74.59	81.41	76.37	59.77	86.69	66.52	84.49	79.01	79.96	74.18	81.22
Mahalanobis	87.09	80.62	70.78	83.79	84.63	73.89	84.15	79.43	83.18	78.83	61.72	84.87	78.59	80.24
kNN+	39.23	92.78	81.34	76.16	80.74	77.58	48.99	89.30	74.99	82.69	57.15	88.35	62.88	84.48
LogitNorm	59.60	90.74	86.73	76.33	80.25	78.58	81.07	82.99	84.19	80.77	86.64	75.60	79.75	80.84
CIDER	23.09	95.16	53.33	88.11	79.63	73.43	16.16	96.33	71.68	82.98	43.87	90.42	46.89	87.67
PALM	3.03	99.23	34.46	93.74	67.80	82.62	10.58	97.70	41.56	91.36	44.06	91.43	33.58	92.68
<b>Ours</b>	<b>2.90</b>	<b>98.86</b>	<b>0.05</b>	<b>97.98</b>	<b>70.55</b>	<b>81.34</b>	<b>12.42</b>	<b>97.06</b>	<b>24.63</b>	<b>94.53</b>	<b>26.49</b>	<b>94.07</b>	<b>22.84</b>	<b>93.97</b>

Table 1: OOD detection performance of various methods using a ResNet-34 backbone, trained on labeled CIFAR-100 as the in-distribution (ID) dataset.  $\downarrow$  ( $\uparrow$ ) indicates that smaller (larger) values are better. **Bold** numbers indicate the best results.

Methods	OOD Datasets													
	SVHN		MNIST		Places365		LSUN		iSUN		Textures		Average	
	FPR95↓	AUROC↑	FPR95↓	AUROC↑	FPR95↓	AUROC↑	FPR95↓	AUROC↑	FPR95↓	AUROC↑	FPR95↓	AUROC↑	FPR95↓	AUROC↑
MSP	59.66	91.25	28.58	94.85	62.46	88.64	51.93	92.73	54.57	92.12	66.45	88.50	53.94	91.35
ODIN	20.93	95.55	69.01	65.23	63.04	86.57	31.92	94.82	33.17	94.65	56.40	86.21	45.74	87.17
Energy	54.41	91.22	32.00	94.58	42.77	91.02	23.45	96.14	27.52	95.59	55.23	89.37	39.23	92.99
Mahalanobis	9.24	97.80	3.45	99.01	83.50	69.56	67.73	73.61	6.02	98.63	23.21	92.91	32.19	88.59
kNN+	2.70	99.61	6.51	98.92	23.05	94.88	7.89	98.01	23.56	96.21	10.11	97.43	12.47	97.51
LogitNorm	45.31	91.98	57.03	88.81	59.69	88.34	50.87	92.44	52.40	90.89	53.78	90.39	53.18	90.48
CIDER	2.89	99.72	19.17	96.99	23.88	94.09	5.75	99.01	20.21	96.64	12.33	96.85	14.04	97.22
PALM	0.52	99.89	2.95	99.39	29.31	94.09	1.78	99.37	27.24	95.67	16.67	97.19	13.08	97.60
<b>Ours</b>	<b>0.51</b>	<b>99.12</b>	<b>2.99</b>	<b>98.81</b>	<b>29.03</b>	<b>94.18</b>	<b>1.86</b>	<b>99.02</b>	<b>27.32</b>	<b>95.65</b>	<b>15.85</b>	<b>96.12</b>	<b>12.93</b>	<b>97.15</b>

Table 2: OOD detection performance of various methods using a ResNet-18 backbone, trained on labeled CIFAR-10 as the in-distribution (ID) dataset.  $\downarrow$  ( $\uparrow$ ) indicates that smaller (larger) values are better. **Bold** numbers indicate the best results.

**Evaluation Metrics.** We evaluate the CER framework and all baseline methods using three standard metrics: (1) **Average FLOPs**: The expected Floating Point Operations per sample during inference, explicitly including the overhead of rejection modules; (2) **FPR95**: The False Positive Rate of OOD data when the ID true positive rate is fixed at 95%; and (3) **AUROC**: The Area Under the Receiver Operating Characteristic curve.

**Model Pre-training.** We employ ResNet-18 for CIFAR-10 and ResNet-34 for CIFAR-100, following the experimental protocols established in [Yang *et al.*, 2022].

**Inference Configuration (CER).** Our method relies on sufficient statistics computed offline using the ID training set. To determine thresholds without data leakage, we randomly partition a held-out ID validation set (10% of the training data). All experiments are conducted on a single NVIDIA L20 GPU.

## 4.2 Experimental Results

CER outperforms a wide range of existing competitive methods. Table 1 summarizes various competitive baselines for OOD detection. All methods are trained on ResNet-34 using CIFAR-100, without assuming access to auxiliary outlier datasets. We compare our method with several recent competitive approaches, including MSP [Hendrycks and Gimpel, 2017], ODIN [Liang *et al.*, 2018], Energy [Liu *et al.*, 2020], Mahalanobis [Lee *et al.*, 2018], kNN+ [Sun *et al.*, 2022], LogitNorm [Wei *et al.*, 2022] CIDER [Ming *et al.*, 2023],

and PALM [Jie and Deng, 2023].

Table 1 shows that CER significantly elevates OOD detection performance. We observe that: (1) Unlike PALM, CER leverages high-frequency asymmetry for early rejection, reducing average FPR95 by 31.98% (from 33.58% to 22.84%) and reaching 93.97% AUROC. (2) CER demonstrates superior robustness on challenging datasets; for instance, it slashes FPR95 on iSUN by 30.01% relative to PALM, proving that physical-level constraints offer vital structural criteria for decision-making. (3) Crucially, CER’s computational efficiency does not compromise accuracy. By integrating high-frequency features with intermediate-layer energy scores, it achieves more discriminative and resource-efficient detection than existing SOTA methods.

As illustrated in Figure4a, to better examine the internal mechanism of CER framework, we visualize the exit distribution of samples for each OOD dataset. For the iSUN dataset, over 60% of the samples are intercepted at the first exit, demonstrating that CER can effectively leverage physical representation features to achieve extremely early anomaly detection. Regarding the MNIST dataset, almost all data are successfully intercepted at the second exit. Furthermore, the orange line representing Computational Savings clearly indicates that the CER framework significantly reduces inference overhead while maintaining robust detection performance.

As evidenced by the comparative data in Table 2, our proposed CER framework challenges the conventional paradigm that computational efficiency inevitably compromises detec-

Method	FLOPS(G) $\downarrow$	Savings. $\downarrow$	AUROC(%) $\uparrow$	FPR(%) $\downarrow$
<b>CIFAR-100</b>				
MSP	1.16	—	—	—
+ CER	<b>0.79 +0.37</b>	<b>31.75%</b>	<b>+18.80</b>	<b>-39.34</b>
ODIN	1.16	—	—	—
+ CER	<b>0.92 +0.24</b>	<b>21.02%</b>	<b>+1.10</b>	<b>-40.78</b>
Energy	1.16	—	—	—
+ CER	<b>0.95 +0.21</b>	<b>17.78%</b>	<b>+9.30</b>	<b>-32.03</b>
kNN+	1.16	—	—	—
+ CER	<b>0.94 +0.22</b>	<b>18.97%</b>	<b>+3.38</b>	<b>-22.4</b>
CIDER	1.16	—	—	—
+ CER	<b>0.95 +0.21</b>	<b>18.36%</b>	<b>+2.57</b>	<b>-17.20</b>
PALM	1.16	—	—	—
+ CER	<b>0.81 +0.35</b>	<b>31.50%</b>	<b>+1.39</b>	<b>-31.98</b>

Table 3: Efficiency and Generalizability Analysis on CIFAR. We report the average computational cost (**FLOPS**), relative savings (**Savings.**), and performance gains in **AUROC** and **FPR** ( $\Delta$  denotes improvement) when integrating CER.

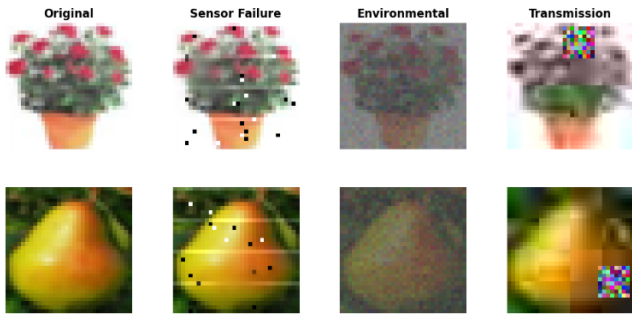


Figure 3: Robustness analysis under extreme environments. The visualization demonstrates the distribution of detection results across different noise and failure scenarios.

tion accuracy. Specifically, CER reduces the average **FPR95** to **12.93%**, effectively surpassing SOTA methods including PALM and CIDER on this critical metric. Despite the introduction of a demand-driven early-exit mechanism, the average **AUROC** of **97.15%** achieved by CER remains highly competitive, with a negligible performance degradation of less than 0.5% compared to the full-path inference of PALM. Combined with the previously observed **20%–30%** reduction in computational cost, these results demonstrate that multi-level feature joint decision-making achieves a superior performance ceiling while maintaining exceptional resource efficiency in complex OOD scenarios.

We present CER as a versatile, plug-and-play enhancer specifically engineered for energy-efficient OOD detection. As evidenced in Table 3, integrating CER as a functional module into mainstream baselines—such as MSP, ODIN, Energy, kNN+, CIDER, and PALM—consistently yields a dual benefit: a substantial reduction in computational overhead alongside a marked improvement in detection robustness.

Though designed for computational efficiency, CER’s multi-exit architecture supports seamless end-to-end train-

Method	Sensor Failure		Environmental		Transmission		Average	
	AUC $\uparrow$	FPR $\downarrow$						
MSP	86.52	61.78	78.08	81.20	76.26	84.40	80.29	75.79
ODIN	67.48	82.12	61.85	88.25	59.50	88.41	62.94	86.26
Energy	92.72	40.13	88.89	66.76	83.10	78.45	88.24	61.78
kNN+	93.16	41.74	89.07	72.72	87.62	66.88	89.95	60.45
CIDER	89.41	70.96	93.03	39.53	73.73	85.42	85.39	66.30
PALM	95.57	25.60	97.87	8.13	88.47	61.25	84.30	48.45
Ours	<b>99.22</b>	<b>3.30</b>	<b>97.29</b>	<b>5.82</b>	<b>91.50</b>	<b>28.25</b>	<b>96.01</b>	<b>12.46</b>

Table 4: Quantitative robustness analysis under extreme environments. We report AUROC (%) $\uparrow$  and FPR95 (%) $\downarrow$  for each scenario.

ing without exhaustive tuning. Our evaluations confirm that CER consistently yields significant computational savings, reducing FLOPs by 17.78%–31.75%. Crucially, these gains are coupled with a substantial boost in detection accuracy (e.g., +18.80% AUROC for MSP) and a drastic reduction in FPR95. These results empirically validate that CER empowers models to bypass redundant feature extractions, reinforcing discriminative precision against OOD samples with a minimal computational footprint.

### 4.3 OOD Detection under Real-World Noise

To evaluate the reliability of the CER algorithm in real-world deployment environments, we constructed the **CIFAR-100-R** robustness benchmark by applying simulated degradations to the complete CIFAR-100 test set. This benchmark is designed to cover a full spectrum of hardware and software failures, ranging from initial sensor acquisition to final network transmission. As illustrated in Figure 3, beyond the original images, we targeted three specific categories of corruption: sensor failure, adverse environmental interference, and transmission-compression loss.

In the Sensor Failure simulation, we focus on the most common defects in CMOS chips—dead pixels and striping noise—to evaluate the model’s robustness against low-level hardware faults. Meanwhile, for Adverse Environments, we simulate visual degradation under extreme weather conditions, utilizing a composite perturbation strategy to faithfully reproduce the contrast loss and color shifts characteristic of dense fog and low-exposure environments. Furthermore, regarding Transmission Loss, we examine the impact of network communication on data quality by combining low-quality encoding with random noise patches to precisely simulate typical keyframe corruption in video streaming.

Table 2 shows that CER outperforms all baselines under extreme stress testing on corrupted datasets. Notably, in the *Sensor Failure* scenario, CER achieves a remarkably low 3.30% FPR95, vastly surpassing Energy-based (40.13%) and PALM (25.60%). Even under severe *Environmental* and *Transmission* degradations, CER maintains robust inference by effectively leveraging residual structural information for accurate detection.

Ultimately, these stress-testing results provide strong evidence that CER possesses high practical value and robustness for real-world deployment scenarios, such as industrial monitoring and autonomous driving, where sensors are prone to

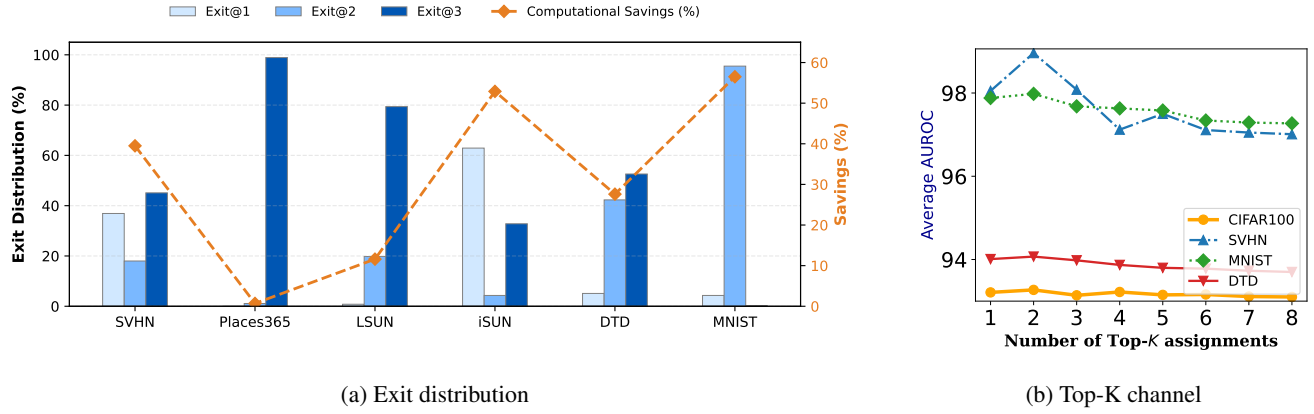


Figure 4: Layer-wise energy analysis for OOD detection. (a) shows the physical frequency filtering at Stage 1, and (b) illustrates the impact of different top- $K$  channel assignments on semantic separation.

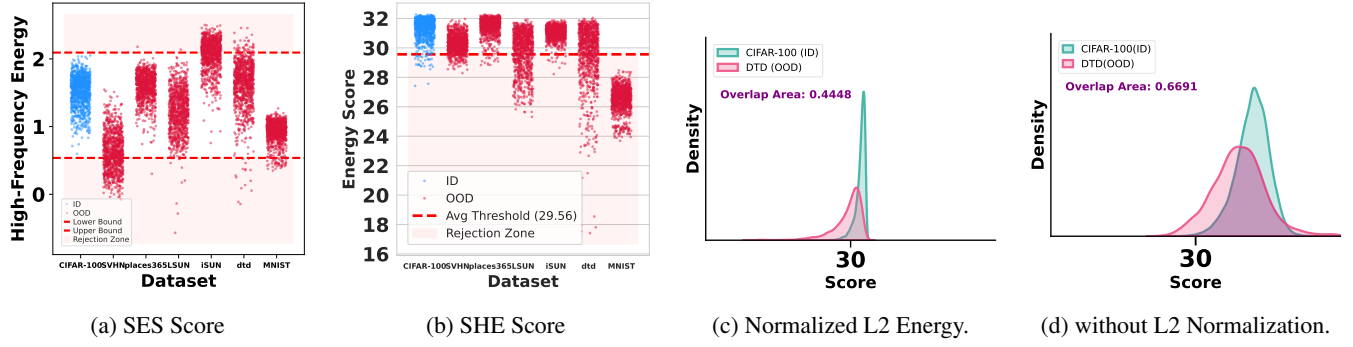


Figure 5: Ablation studies on different components of our method.

diverse external interferences.

#### 4.4 Ablation Studies

Selecting top-tier channels yields significant performance gains. As illustrated in Fig 4b, within the high-frequency energy components, we observe that the AUROC exhibits a gradual declining trend as the value of  $K$  (i.e., the number of selected channels) further increases. This indicates that incorporating excessive low-energy channels introduces irrelevant physical details, which inevitably interferes with the SHE module's capability to capture semantic misalignments.

The synergy between SES and SHE underpins CER's robustness. As illustrated in Fig. 5a, SES acts as a first-line defense, intercepting physical anomalies (e.g., iSUN) via high-frequency energy. While SES's power is limited for semantic-shift datasets like MNIST, Fig. 5b shows that SHE fills this gap through adaptive semantic clustering. This hierarchical collaboration ensures that physical noise and semantic shifts are addressed at their respective levels, achieving exceptional performance.

**Dataset-Specific Gains of L2 Normalization.** Our ablation analysis reveals that L2 normalization yields substantial performance gains specifically for datasets with significant semantic shifts, such as MNIST and DTD. As illustrated in

the contrast between Fig. 5c and Fig. 5d, for DTD, the application of normalization collapses the ID distribution into a compact peak, effectively reducing the overlap area from 0.67 to 0.44. This indicates that by projecting features onto a hypersphere, the SHE module can focus on angular distinguishability while ignoring magnitude-induced noise. For other datasets where the distribution shifts are less semantically distinct, the impact of L2 normalization is relatively moderate, confirming its specialized role in resolving complex semantic misalignments that bypass the initial physical-layer filtering.

## 5 Conclusion

In this study, we propose the Cascaded Early Rejection (CER) framework, a novel hierarchical inference paradigm designed to rectify the pervasive issues of computational mismatch and semantic hallucination in Out-of-Distribution (OOD) detection. CER optimizes the detection pipeline by thoroughly decoupling shallow signal rejection from deep semantic discrimination. Through the synergy of the SES and SHE modules, our framework not only significantly reduces computational overhead but also enhances overall detection performance. Notably, CER demonstrates superior early interception capabilities in safety-critical scenarios involving sensor

failures and environmental noise, setting a new benchmark for reliable and energy-efficient OOD deployment at the edge.

## References

- [Bernhard and others, 2021] M. Bernhard et al. Impact of low-pass filtering on out-of-distribution detection. In *Proceedings of the IEEE/CVF International Conference on Computer Vision (ICCV)*, 2021.
- [Chen and Wang, 2025] Y. Chen and H. Wang. Decoupling physical and semantic shifts: A frequency-domain perspective for robust out-of-distribution detection. In *International Conference on Learning Representations (ICLR)*, 2025.
- [Cimpoi et al., 2014] Mircea Cimpoi, Subhransu Maji, Iasonas Kokkinos, Sammy Mohamed, and Andrea Vedaldi. Describing textures in the wild. In *Proceedings of the IEEE Conference on Computer Vision and Pattern Recognition*, pages 3606–3613, 2014.
- [Djurisic et al., 2023] Andrija Djurisic, Aleksandar Bojchevski, Izabela Vorsam, and Stephan Günnemann. Out-of-distribution detection with activation shaping. In *International Conference on Learning Representations (ICLR)*, 2023.
- [Hasnat et al., 2017] Md Abul Hasnat, Jean-Philippe Bohné, Jonathan Milgram, Stephane Gentric, and Liming Chen. von mises-fisher mixture model-based deep learning: Application to face verification. In *Proceedings of the European Conference on Computer Vision (ECCV)*, 2017.
- [Hendrycks and Gimpel, 2017] Dan Hendrycks and Kevin Gimpel. A baseline for detecting misclassified and out-of-distribution examples in neural networks. In *International Conference on Learning Representations (ICLR)*, 2017.
- [Huang et al., 2018] Gao Huang, Danlu Chen, Tianhong Li, Felix Wu, Laurens van der Maaten, and Kilian Q Weinberger. Multi-scale dense networks for resource efficient image classification. In *International Conference on Learning Representations (ICLR)*, 2018.
- [Huang et al., 2021] Rui Huang, Andrew Geng, and Yixuan Li. Mos: Towards scaling out-of-distribution detection for large semantic bins. In *Proceedings of the IEEE/CVF Conference on Computer Vision and Pattern Recognition (CVPR)*, pages 13910–13919, 2021.
- [Jie and Deng, 2023] Shuo Jie and Zhijie Deng. Learning with mixture of prototypes for out-of-distribution detection. In *International Conference on Machine Learning (ICML)*, 2023.
- [Kaya et al., 2019] Yigit Kaya, Sanghyun Hong, and Tudor Dumitras. Shallow-deep networks: Understanding and mitigating network overthinking. In *Proceedings of the 36th International Conference on Machine Learning (ICML)*, pages 3301–3310. PMLR, 2019.
- [Krizhevsky et al., 2009] Alex Krizhevsky, Geoffrey Hinton, et al. Learning multiple layers of features from tiny images. *Master's thesis, University of Toronto*, 2009.
- [LeCun et al., 1998] Yann LeCun, Léon Bottou, Yoshua Bengio, and Patrick Haffner. Gradient-based learning applied to document recognition. *Proceedings of the IEEE*, 86(11):2278–2324, 1998.
- [Lee et al., 2018] Kimin Lee, Kibok Lee, Honglak Lee, and Jinwoo Shin. A simple unified framework for detecting out-of-distribution samples and adversarial attacks. In *Advances in Neural Information Processing Systems*, volume 31, 2018.
- [Li and others, 2023] J. Li et al. Rethinking early exiting for efficient and reliable predictions. In *Proceedings of the IEEE/CVF International Conference on Computer Vision (ICCV)*, 2023.
- [Liang et al., 2018] Shiyu Liang, Yixuan Li, and R Srikant. Enhancing the reliability of out-of-distribution image detection in neural networks. In *International Conference on Learning Representations (ICLR)*, 2018.
- [Lin et al., 2021] Ziqian Lin, Bin Pang, Siyuan Liang, et al. Mood: Multi-level out-of-distribution detection. In *Proceedings of the IEEE/CVF Conference on Computer Vision and Pattern Recognition*, pages 15313–15323, 2021.
- [Liu et al., 2020] Weitang Liu, Xiaoyun Wang, John Owens, and Yixuan Li. Energy-based out-of-distribution detection. In *Advances in Neural Information Processing Systems (NeurIPS)*, 2020.
- [Ming and Li, 2023] Yifei Ming and Yixuan Li. How to rely on your model: A geometry-aware calibration for out-of-distribution detection. In *Proceedings of the IEEE/CVF Conference on Computer Vision and Pattern Recognition (CVPR)*, 2023.
- [Ming et al., 2023] Yifei Ming, Yiyou Sun, Oulu Gu, Stephen Fienberg, and Yixuan Li. How to exploit hyperspherical embeddings for out-of-distribution detection? In *International Conference on Learning Representations (ICLR)*, 2023.
- [Netzer et al., 2011] Yuval Netzer, Tao Wang, Adam Coates, Alessandro Bissacco, Bo Wu, and Andrew Y Ng. Reading digits in natural images with unsupervised feature learning. *NIPS Workshop on Deep Learning and Unsupervised Feature Learning*, 2011.
- [Nguyen et al., 2015] Anh Nguyen, Jason Yosinski, and Jeff Clune. Deep neural networks are easily fooled: High confidence predictions for unrecognizable images. In *Proceedings of the IEEE conference on computer vision and pattern recognition (CVPR)*, pages 427–436, 2015.
- [Peng et al., 2025] Ningkang Peng, Yuzhe Mao, Yuhao Zhang, Linjin Qian, Qianfeng Yu, Yanhui Gu, Yi Chen, and Li Kong. A multi-dimensional semantic surprise framework based on low-entropy semantic manifolds for fine-grained out-of-distribution detection. *arXiv preprint arXiv:2510.13093*, 2025.
- [Scardapane et al., 2020] Simone Scardapane, Michele Scarpiniti, Enzo Baccarelli, and Aurelio Uncini. Differentiable branching in deep networks for fast inference. *IEEE Transactions on Neural Networks and Learning Systems*, 31(10):4100–4111, 2020.

- [Smith and Li, 2025] J. Smith and Y. Li. Geometric constraints for hyperspherical ood detection. In *Proceedings of the IEEE/CVF Conference on Computer Vision and Pattern Recognition (CVPR)*, 2025.
- [Sun *et al.*, 2021] Yiyou Sun, Chuan Guo, and Yixuan Li. React: Out-of-distribution detection with rectified activations. In *Advances in Neural Information Processing Systems (NeurIPS)*, volume 34, pages 144–157, 2021.
- [Sun *et al.*, 2022] Yiyou Sun, Yifei Guo, and Yixuan Li. Out-of-distribution detection with deep nearest neighbors. In *International Conference on Machine Learning (ICML)*, 2022.
- [Teerapittayanon *et al.*, 2016] Surat Teerapittayanon, Bradley McDanel, and Hsiang-Tsung Kung. Branchynet: Fast inference via early exiting from deep neural networks. In *2016 23rd International Conference on Pattern Recognition (ICPR)*, pages 2464–2469. IEEE, 2016.
- [Wang and Zhang, 2025] Li Wang and Wei Zhang. Geometric consistency on hyperspheres for robust ood detection. In *Proceedings of the IEEE/CVF Conference on Computer Vision and Pattern Recognition (CVPR)*, 2025.
- [Wang *et al.*, 2020] Haohan Wang, Xindi Huang, Zixuan Wu, and Eric P Xing. High-frequency component helps explain the generalization of cnns. In *Proceedings of the IEEE/CVF Conference on Computer Vision and Pattern Recognition (CVPR)*, pages 8684–8694, 2020.
- [Wei *et al.*, 2022] Hongxin Wei, RENCHUNZI Xie, Hao Cheng, Lei Feng, Bo An, and Yixuan Li. Mitigating neural network overconfidence with logit normalization. *arXiv preprint arXiv:2205.09310*, 2022.
- [Wolczyk and others, 2021] M. Wolczyk et al. Zero time waste: An early exit network for real-time ood detection. In *Proceedings of the IEEE/CVF Conference on Computer Vision and Pattern Recognition (CVPR)*, 2021.
- [Xu *et al.*, 2015] Pingmei Xu, Krista A Ehinger, Yinda Zhang, Adam Finkelstein, Sanjeev R Kulkarni, and Jianxiong Xiao. Turkergaze: Crowdsourcing saliency with webcam based eye tracking. In *arXiv preprint arXiv:1504.06755*, 2015.
- [Yang *et al.*, 2022] Jingkang Yang, Kaiyang Zhou, Yixuan Li, and Ziwei Liu. Openood: Benchmarking generalized out-of-distribution detection. In *Advances in Neural Information Processing Systems (NeurIPS)*, 2022.
- [Yu *et al.*, 2015] Fisher Yu, Ari Seff, Yinda Zhang, Shuran Song, Thomas Funkhouser, and Jianxiong Xiao. Lsun: Construction of a large-scale image dataset using deep learning with humans in the loop. *arXiv preprint arXiv:1506.03365*, 2015.
- [Zeiler and Fergus, 2014] Matthew D Zeiler and Rob Fergus. Visualizing and understanding convolutional networks. In *European conference on computer vision (ECCV)*, pages 818–833, 2014.
- [Zhou *et al.*, 2017] Bolei Zhou, Agata Lapedriza, Aditya Khosla, Aude Oliva, and Antonio Torralba. Places: A 10 million image database for scene recognition. *IEEE Transactions on Pattern Analysis and Machine Intelligence*, 40(6):1452–1464, 2017.